Surface & Coatings Technology 418 (2021) 127232

Contents lists available at ScienceDirect

Surface & Coatings Technology

journal homepage: www.elsevier.com/locate/surfcoat

Electrophoretically deposited high molecular weight chitosan/bioactive glass composite coatings on WE43 magnesium alloy

Agnieszka Witecka [a,b,*], Svenja Valet [b], Michał Basista [a], Aldo Roberto Boccaccini [b,**]

[a] Institute of Fundamental Technological Research, Polish Academy of Sciences, Pawińskiego 5B Street, 02-106 Warsaw, Poland
[b] Institute of Biomaterials, Department of Materials Science and Engineering, University of Erlangen-Nuremberg, Cauerstrasse 6, 91058 Erlangen, Germany

ARTICLE INFO

Keywords:
WE43
Magnesium alloy
Chitosan
Bioactive glass
Mesoporous nano bioactive glass
Electrophoretic deposition

ABSTRACT

Mg-based materials are good candidates for biodegradable bone regeneration implants due to their favorable mechanical properties and an excellent compatibility with human bone. However, too high corrosion/degradation rate in body fluids still limits their applicability. Coatings based on chitosan (CS) and bioactive glass (BG) particles fabricated by electrophoretic deposition (EPD) on Dulbecco's Modified Eagle Medium (DMEM) pre-treated magnesium alloys have promising potential to suppress the substrate corrosion and additionally to incorporate bioactivity. However, the impact of processing parameters or type of coating components on the long-term substrate corrosion behavior and cell response have not been investigated previously. In this study, two types of composite coatings based on a high molecular weight CS (M_w 340–360 kDa, DDA $\geq$ 95%) and embedded particles: solid BG (2 μm) and a mixture of BG and mesoporous bioactive glass nanoparticles (MBGN, 100–300 nm with mesopores 2.3–5.6 nm) were fabricated by EPD on DMEM pre-treated WE43 magnesium alloy. It was found that partial replacement of BG particles with MBGN (ratio 3:1) in the composite coating increases the water contact angle, surface roughness and induces a positive cell response. Although the acidic CS-based solutions and applied EPD conditions may decrease the stability of the temporary barrier formed during the DMEM pre-treatment on WE43 substrate therewith slightly increasing its corrosion sensitivity, the composite coating with a mixture of different sizes of particles (BG, MBGN) is a promising candidate for bone regeneration applications.

1. Introduction

Mg-based materials are suitable candidates for temporary, biodegradable medical applications such as implants and tissue scaffolds [1,2] because of their biocompatibility [1,3,4], biodegradability [5–7] and excellent mechanical properties similar to those of cortical bone [4]. Mg is an essential ion in the human body with expected low toxicity, due to its efficient excretion through the urinary system [8]. However, as Mg is prone to strong corrosion, an excessive corrosion of Mg-based materials may negatively influence the healing process or even cause failure of the implant [1,2,9]. In the presence of moisture Mg undergoes corrosion (Eq. (1)):

$$Mg + 2H_2O \rightarrow Mg^{2+} + 2OH^- + H_2\uparrow \quad (1)$$

Besides the release of Mg^{2+}, the corrosion process is accompanied by H_2 generation, which in high amount results in gas pocket formation [7] and by OH^- release, which may reduce cytocompatibility through local alkalization [4]. Furthermore, a high pH leads to formation of $Mg(OH)_2$ on the surface that may act as a temporary barrier for further corrosion in certain conditions. Fluctuations of pH strongly influence the corrosion sensitivity of Mg-based materials, as they have impact on the stability of the temporary barrier [10–12]. Because corrosion of Mg in the human body is more complex than in H_2O due to the presence of organic and inorganic compounds, living cells, dissolved O_2 or CO_2, which provide a strong buffering effect and may affect the implant response [12,13], it is important to maintain a similar pH level in *in vitro* experiments.

Available strategies for decreasing the corrosion rate of Mg include: a) purification and alloying [14], b) tailoring of the microstructure [6,12], and c) surface modification, specially the application of protective and/or bioactive coatings [15–17]. The ideal strategy should lead to the decrease of the corrosion process instead of its complete stoppage.

* Correspondence to: A. Witecka, Institute of Fundamental Technological Research, Polish Academy of Sciences, Pawińskiego 5B Street, 02-106 Warsaw, Poland.
** Corresponding author.
E-mail addresses: awitecka@ippt.pan.pl (A. Witecka), aldo.boccaccini@fau.de (A.R. Boccaccini).

https://doi.org/10.1016/j.surfcoat.2021.127232
Received 1 March 2021; Received in revised form 20 April 2021; Accepted 21 April 2021
Available online 29 April 2021

Application of a biodegradable polymer-based coatings [18,19] is a promising strategy for controlling the corrosion of Mg-based implants by corrosion rate to the rate of the surrounding tissue healing, without changing the bulk mechanical properties. Moreover, the modification of surface properties can increase the implant biocompatibility, e.g. by adding extra functionalities, such as the release of stimulating substances from the applied coating [20] or by inducing a surface topography suitable for cell adhesion [21]. Therefore, the appropriate selection of biodegradable polymers and additives is crucial.

This paper focuses on the development of chitosan (CS)/bioactive glass (BG) composite coatings via electrophoretic deposition (EPD) on WE43 magnesium alloy with the far-reaching goal of obtaining a suitable material for biodegradable implants.

EPD is a versatile and cost-effective coating technique [22] for deposition or co-deposition of different materials [23], including biological entities [24], variety of biopolymers or bioactive and functional composite coatings [23,25,26] on corrosion resistant metals such as titanium [27] and stainless steel [28], but also on corrosion sensitive substrates such as Mg-based materials [28,29]. A typical component of functional coatings used in bone regeneration is BG, due to its ability to form a hydroxyapatite (HA) layer on its surface [30] and extra biological activity provided by the release of biologically active ions [31]. Various chemical compositions, sizes or shapes (spherical, non-spherical) of BG particles, including mesoporous nanoparticles [32], affect their physicochemical and biological properties for specific biomedical applications. Nowadays, nano size BG particles are increasingly used due to their higher specific surface area in comparison with micro size BG particles, facilitating HA formation during the exposure to body fluids. A larger surface to volume ratio may facilitate nano sized BG particles integration with polymer matrix. Incorporation of such nanoparticles into a thin coating induces a nanostructured topography on the surface, which may result in higher protein adsorption ability. Nano size mesoporous BG particles (MBGN) additionally provide an increase of porosity, which is useful for the delivery of therapeutic molecules for hard and soft tissue repair [33]. The use of both of micro and nano sized BG particles instead of only single size BG particles may bring additional benefits to the functional coating resulting from specific particle properties (e.g. increase in surface topography, different rate of HA nucleation, additional sites for HA nucleation located between micron size BG particles). BG and MBGN particles simultaneously incorporated in composite coatings by EPD have not been extensively considered before.

From a technical point of view, for the fabrication of polymer based composite coating with embedded particles via EPD on a Mg-based substrate, it is preferable to choose a polymer, which can form a liquid cationic polyelectrolyte, so that bonding between polymer molecules and negative charged particles is possible facilitating also the assembly of uniform coating. CS, due to its unique physicochemical properties, fulfills this condition. Additionally, CS is suitable for cathodic EPD and this process can be successfully applied for Mg-based materials, because the anode, not the cathode, undergoes intensive dissolution in the EPD cell.

In CS + BG type of composite coatings, CS plays the role of the matrix for BG particles to ensure their attachment to the metallic substrate [29]. Indeed, in the composite, CS works as a "glue" for the embedded particles, omitting the sintering step which is essential for pure ceramic coatings. As the working temperature for Mg-based materials is low (≤400 °C), the use of high temperature processes has limitations, thus the chosen, room temperature, approach is justified. Additionally, the CS matrix effectively controls the dissolution rate of BG particles in the composite coating and the corrosion rate of corrosion sensitive substrates such as Mg-based materials, because of the slower CS degradation profile. CS is a valuable polymer for biomedical applications because of its biodegradability, biocompatibility and antimicrobial activity [20,34–36]. However, swelling, solubility, biodegradation and film forming of CS depend on its structure, including its molecular weight (M_w) and degree of deacetylation (DDA) [37]. CS is a copolymer composed of *N*-acetyl-D-glucosamine and D-glucosamine units obtained by partial deacetylation of chitin. The ratio between the two units corresponds to % of DDA and determines the number of chemical reactive amino groups along the chain. A high DDA can be associated with more regular packing of the polymer chains in the structure which directly influences the properties of the coating. CS dissolution in acidic solution (pH < 6) leads to protonation of its amino groups and formation of a cationic polyelectrolyte suitable for EPD (Eq. (2)) [38]:

$$CS - NH_2 + H_3O^+ \rightarrow CS - NH_3^+ + H_2O \quad (2)$$

$$2H_2O + 2e^- \rightarrow H_2\uparrow + 2OH^- \quad (3)$$

$$CS - NH_3^+ + OH^- \rightarrow CS - NH_2 + H_2O \quad (4)$$

During the EPD process, the applied electric field between the electrodes provides electrophoretic movement of positively charged CS molecules towards the cathode, while during the co-deposition of both CS molecules and BG particles CS serve as a surface charging agent for the BG particles. Hydrogen bonding between the hydroxyl and amine groups of CS and the hydroxyl groups of BG causes adsorption of CS molecules on the BG particles and thus movement of both components towards the cathode. The higher pH at the cathode, caused by H_2O decomposition (Eq. (3)), triggers a charge loss of CS molecules (pH ≥ 6.5), which leads to the formation of an insoluble CS-based deposit on the cathode surface (Eq. (4)). However, immersion of Mg-based substrates in an acidic EPD suspension (corrosive environment) and any pH fluctuations close to its surface, may negatively affect its corrosion rate. The H_2 generated by the EPD process (Eq. (3)) and the corrosion reaction (Eq. (1)) can be entrapped in the fabricated deposit and negatively influence its quality. Hence, for the deposition of a uniform coating on Mg-based substrates via EPD, the metal corrosion rate needs to be suppressed, for instance by a surface DMEM pre-treatment [29,39,40].

Heise et al. [29] fabricated via EPD a medium M_w CS + BG composite coating on DMEM pretreated WE43 magnesium alloy substrates and evaluated their corrosion behavior, indicating an important role of the pretreatment in controlling the degradation of the Mg-based substrates and the deposition of the composite coating via EPD. The authors pointed out that an in-depth investigation of the long-term corrosion protection provided by the CS + BG coatings is needed. Also, the impact of different coating characteristics should be considered (e.g. type of CS, BG content) on the corrosion protection capability and cell biology performance of the coatings. Due to the important role of a pre-treated surface, limitation of the substrate corrosion during the coating deposition via EPD needs to be considered by modification of the EPD parameters (e.g. deposition time and/or applied potential). Additionally, changes in the coating components (e.g. type of CS or BG particles) may affect its homogeneity.

Most of the studies related to CS + BG coatings deposited via EPD have been carried out on corrosion resistant substrates [41–44], while the effect of the M_w or DDA of the CS was not always investigated [27,41–43,45,46]. For corrosion sensitive substrates such as Mg-based materials, only medium M_w CS (190–310 kDa) with ~85% DDA [28,29,40,47] has been used, while no research has been conducted on the application of CS with high M_w and DDA in EPD coatings. Also, the effects of different sizes and morphologies of BG particles have not been investigated.

Therefore, the aim of this study is (i) to deposit high M_w CS-based bioactive composite coatings containing bioactive particles via EPD on pre-treated WE43 substrate and (ii) to examine the coatings properties and performance, including cell response and substrate corrosion under cell culture conditions. For this purpose, two types of composite coatings were deposited using high M_w CS (340–360 kDa) with DDA ≥ 95% and different bioactive glass particles: microparticles (non-spherical, dense) and a mixture of microparticles and nanoparticles (spherical, mesoporous).

2. Materials and methods

The CS solution for EPD was prepared by adding 0.5 g/L of CS (DDA ≥ 95%, M_w 340–360 kDA, ChitoClear, Primex) to 20 vol% deionized water, 1 vol% acetic acid (Sigma Aldrich) and 79 vol% of pure ethanol (Emsure, Merck). The glass content in the EPD suspensions was set to 1 g/L based on previous studies on medium M_w CS-based solutions [29]. Two types of bioactive glass particles were used: 1) commercial melt-derived 45S5 bioactive glass particles (BG; Vitryxx®, Schott AG, Germany) with composition in wt%: 45 SiO_2, 24.5 CaO, 24.5 Na_2O, 6 P_2O_5, non-spherical shape [28] with median diameter of 2 μm (the size analysis of particles provided by the supplier indicated that 10% of the particles were below 0.3 μm, 50% below 2 μm, and 99% below 5 μm); 2) mesoporous bioactive glass nanoparticles (MBGN), obtained by the microemulsion-assisted sol-gel method, with nominal composition in mol%: 70 SiO_2, 30 CaO (chemical composition calculated based on EDX data in mol%: 86.1 ± 0.3 SiO_2, 13.9 ± 0.2 CaO), spherical shape with size range of 100–300 nm (specific surface area 381 m^2/g) and mesopores throughout the nanoparticle (pore size distribution 2.3–5.6 nm and pore volume 0.7 cm^2/g) [33]. The BG particles or a mixture of BG particles and MBGN in ratio 3:1, which yielded the best coating homogeneity in preliminary trial-error tests, were added to the polymer matrix. In what follows, the deposited composite coatings are abbreviated as CS + BG (CS and 1 g/L BG particles) and CS + MIX (CS and 0.75 g/L BG/0.25 g/L MBGN particles), respectively. Before deposition the suspensions were magnetically stirred for 5 min, followed by 45 min of ultrasonication (Sonorex RK 100, Bandelin electronic GmbH & Co. KG) to obtain an adequate dispersion of the particles in the suspension. Disc-shaped WE43 magnesium alloy (4 wt% Y, 3 wt% Nd, Mg-bal.) samples with a diameter of 10 mm and a height of 4 mm were ground up to 1200 grid (Buehler GMbH), ultrasonically cleaned in pure ethanol (VWR Chemicals) and blow dried with nitrogen. Such prepared WE43 samples were pre-treated in Dulbecco's Modified Eagle's Medium (DMEM, Sigma Aldrich, Life Science) for 24 h under constant stirring at room temperature to allow the formation of the temporary barrier on the surface. These pre-treated WE43 samples were used as the working electrodes (deposition area 69.4 mm^2), while AISI 316L stainless steel foils (Thyssenkrupp AG) with dimensions of 15x30x0.2 mm^3 (immersed: 15x15x0.2 mm^3) were used as counter electrodes for direct current EPD. The distance between the electrodes in the EPD cell was set to 1 cm. The coated samples were air-dried overnight and weighted with an accuracy of 0.0001 g. For a comparative study of the amount of coating, the deposit yields of the coatings (deposition weight per surface, D_w) on the pre-treated WE43 substrates (with the same applied voltage and time as CS + BG and CS + MIX) were evaluated based on the formula (Eq. (5)):

$$D_w = (W_d - W_{initial})/S_o \quad (5)$$

where W_d is the weight of the dry sample after EPD, $W_{initial}$ is the weight of the dry sample before EPD, and S_o is the coated surface area. The stability of the dispersed particles in the suspension was determined by zeta-potential (ZP) measurements performed using a Zetasizer Nano ZS (Malvern Instruments, UK). The BG content for ZP measurements was kept at 0.1 g/L. To reveal the grains of the WE43 alloy, samples were polished up to 1 μm, etched by Nital and observed under optical microscope (Zeiss Axioscope) and scanning electron microscopy (SEM, TM1000, Hitachi). Deposited coatings were characterized by SEM (Auriga-4750, Zeiss). Surface roughness was examined with a laser profilometer (UBI Microfocus Expert) according to DIN EN ISO 4768. Every sample was measured 3 times with a measured length of 3 mm and 1000 P/mm. Fourier transform infrared spectroscopy (FTIR) (Nicolet 8700, Thermo Scientific, USA) in the mid-IR region 4000–400 cm^{-1} (40 scans with a resolution of 8 cm^{-1}, ATR-FTIR mode with diamond crystal) was used to confirm the composition of the coating. Contact angle measurements (WCA) were performed (DSA 30 Kruess, Germany) in a static mode using deionized water droplets. Corrosion studies were performed at room temperature in 0.1 M NaCl (Sigma Aldrich) after 1 h immersion in solution while monitoring open circuit potential (OCP), using a VMP 3 multichannel potentiostat/galvanostat (BioLogic, Science Instruments, France). A three electrodes system consisting of an Ag/AgCl (sat. KCl) electrode as reference electrode, Pt electrode (50 mm^2) as counter electrode and a sample (exposed area of 0.264 cm^2) as working electode was used. Electrochemical impedance spectroscopy (EIS) was performed at the OCP with an AC amplitude of 5 mV in the frequency range of 10^{-2}–10^5 Hz. Potentiodynamic measurements were performed at a scanning rate of 0.5 mV/s with potential from −0.3 V in relation to the OCP in anodic direction. Corrosion rate (I_{corr}) was evaluated from the polarization curves by the Tafel method using a software EC-lab V11.25 (BioLogic, Science Instruments, France).

2.1. Cell experiments

2.1.1. Cell proliferation

To determine the cell response to reference (pre-treated, pure CS coated) and composite coated (CS + BG, CS + MIX) samples, tests with stromal cell line ST-2, derived from mouse bone marrow were performed. All types of samples were placed separately into 24-well plates and sterilized under ultraviolet (UV) light for 2 h. ST-2 cells were inoculated at a density of 50.000 cells/mL in 1 mL of Dulbecco's Modified Eagle's Medium (DMEM) supplemented with 10% (v/v) fetal bovine serum (FBS) and 1% (v/v) penicillin-streptomycin (P/S; Gibco, Life Technologies™) on the tested samples and into wells without samples [positive control (+)] and then 24-well plates were incubated under cell culture conditions (37 °C, 5% CO_2) up to 7 d. The culture medium (DMEM+10%FBS + 1%PS) was exchanged every 48 h. Next, the alamarBlue® assay (Invitrogen Corporation) was implemented. The well plates with the samples, positive control (+) and negative control (−) [well without cells], were washed with 1 mL of phosphate-buffered saline (PBS, Gibco, Life Technologies™). Then, PBS was replaced by 1 mL of DMEM + 10%FBS + 1%PS containing 10% (v/v) alamarBlue® and the well plates were incubated for 4 h under cell culture conditions (37 °C, 5% CO_2). Afterwards, 100 μL portions of the supernatants were poured into a 96-well plate and the absorbance of the supernatants was measured at 570 nm and 600 nm. The alamarBlue® contains an oxidation-reduction colorimetric indicator. Its chemical reduction is used for the detection of cells' metabolic activity.

2.1.2. Cell functionality

To determinate the impact of the composite coatings on the relative alkaline phosphatase activity (ALP), reference (pre-treated, pure CS-coated) and composite coated (CS + BG, CS + MIX) samples were incubated up to 16 days with ST-2 cells under cell culture conditions (37 °C, 5% CO_2). Cells were seeded on the samples surface at a density of 30.000 cells/cm^2. For this study the cell culture medium RPMI 1640 w/o phenol red+10% FBS + 1% PS was used. After 4 d of incubation the culture medium was exchanged into osteogenic differentiation medium (culture medium supplemented by 50 μL/mL of ascorbic acid, 10 mmol of β-glycerolphosphate and 10 nM of dexamethasone). The samples were incubated in this medium for additional 3, 6 and 12d, while it was exchanged every 2 d. For clarity, these time points were marked on the graphs as 7 d, 10 d and 16 d, respectively. At the designed time points, the tested samples and controls were subjected to ALP assay. The samples were transferred into a new 24-well plate and the cells were lysed by lysis buffer for 30 min. Collected cell lysis was centrifuged for 5 min at 2000 rpm and then ALP activity was examined using a procedure provided by the Institute of Biomaterials at University of Erlangen-Nuremberg. Briefly, the cell lysis from each sample (250 μL) was incubated with a buffer solution (100 μL) containing 0.1 M Tris, 2 mM $MgCl_2$, 9 mM para-Nitrophenylphosphate (p-NPP) and ultrapure water. In the presence of ALP the enzyme p-NPP is transformed into p-NP (para-Nitrophenol + phosphate). After 180 min of incubation at 37 °C, the color of the liquid became yellowish and the reaction was stopped with

650 μL of 1 M NaOH solution. Then, absorption was measured at 405 and 690 nm using a UV–Vis spectrometer (Specord 40, Analytik Jena, Germany). The protein concentration in the cell lysis was determined by Bradford protein assay (PanReac AppliChem, Germany) by mixing 25 μL of cell lysis with 975 μL of Bradford reagent and measuring the absorbance at 595 nm after 10 min of incubation. The ALP activity was expressed as nmol of converted p-nitrophenol per min and normalized with respect to the protein concentration present in the cell lysis. The relative ALP activity was expressed as nmol p-nitrophenol per min per mg protein.

2.1.3. Weight loss

Air-dried pre-treated and coated (pure CS, CS + BG, CS + MIX) samples, which remained after cell functionality tests were subjected to chromic acid cleaning to remove residues of cells, coatings and insolube salt layers formed on the sample surfaces. Every sample was immersed separately in the cleaning solution (mixture of 20 g of CrO_3 and 1 g of $NaNO_3$ in 100 mL of distilled water) for 3 min at room temperature and rinsed in destilled water. The excess water was gently removed and samples were left to air-dry. Samples weight loss (W_{loss}) was obtained from the following formula (Eq. (6)):

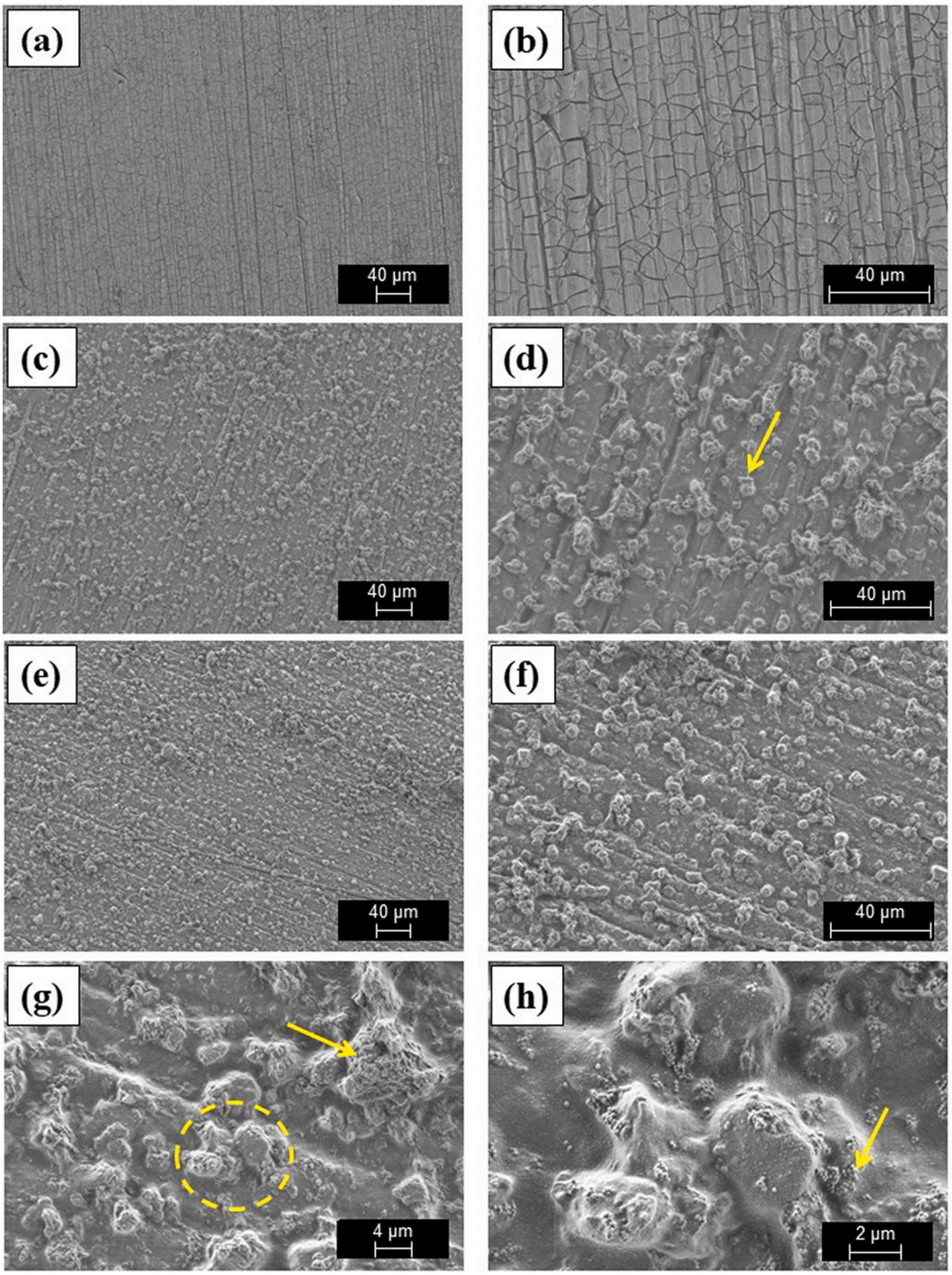

Fig. 1. SEM images of the samples surfaces: (a–b) pre-treated WE43 substrate, (c–d) deposited CS + BG composite coating, (e–f) deposited CS + MIX composite coating, (g–h) BG and MBGN distribution in the CS + MIX coating. Yellow arrows indicate BG particles in (d) and MBGN particles in (g–h), while the yellow circle highlights the magnified area in (h).

$$W_{loss} = (W_{initial} - W_{remain})/S_0 \quad (6)$$

where $W_{initial}$ and S_0 denote the initial weight (after pre-treatment, before EPD) and the total area of the sample, respectively, and W_{remain} is the weight of the sample after chromic acid cleaning. Surface morphology after chromic acid cleaning and Au sputtering was observed by SEM (Phenom proX desktop, ThermoFisher Scientific).

2.2. Statistics

Statistical analyses were performed by one-way ANOVA together with a multi-comparison by Tukey test.

3. Results

3.1. Coating characterization

3.1.1. Morphology of composite coatings

The surfaces of pre-treated WE43 and composite coated (CS + BG, CS + MIX) samples at different magnifications are presented in Fig. 1. The best quality composite coatings in terms of homogeneity were obtained at 50 V and 60 s as deposition voltage and time, respectively. Both types of composite coatings form continuous cover on the pre-treated surfaces, while the BG particles are homogeneously embedded in the CS matrix. Partial replacement of micro size BG particles with nano size MBGN particles in the CS + MIX coating resulted in filled spaces between the larger BG particles or the presence of single MBGN particles and their agglomerates (even larger than 2 μm) on top of the BG particles (Fig. 1g–h). However, for both types of composite coatings, polishing marks from the substrate surfaces were still noticeable.

3.1.2. Zeta potential

Table 1 presents the ZP values obtained for the micron size BG particles and the mixture of micrometric BG and nanosized MBGN particles (ratio 3:1) suspended in CS solution. Both ZP values have positive sign, which indicates cathodic deposition via EPD. Moreover, the value of the ZP for the mixture of particles (CS + MIX) is higher than for pure micron size particles (CS + BG).

3.1.3. Deposit weight

For the same processing parameters (50 V, 60 s), the D_w of the deposited coatings (CS, CS + BG, CS + MIX) slightly differs from each other (Table 1), manifesting higher values for the composite coatings. Additionally, the D_w is slightly higher for the CS + MIX coating than the CS + BG coating.

3.1.4. Surface roughness

The presence of particles (BG, MBGN) in the composite coatings increases the maximum roughness (R_{max}) of the pre-treated WE43 substrate, while the average surface roughness (R_a) slightly differes among samples (Table 1). The CS + MIX coating exhibited a higher R_{max} than the CS + BG.

3.1.5. WCA

The static water contact angle (WCA) differs among the pre-treated WE43 and the coated (pure CS, CS + BG, CS + MIX) samples (Table 1). As expected, the presence of coatings changes the wettability of the pre-treated WE43 substrate depending on the coating components: towards more hydrophobic for the pure CS coating and more hydrophilic for the composite coatings. However, the CS + BG coating shows a slightly higher wettability than the CS + MIX coating.

Table 1
Characteristics of particles, coatings and the surfaces of the samples.

Sample	ZP [mV]	D_w [mg/cm^2]	R_a [μm]	R_{max} [μm]	WCA [°]
Pre-treated	–	–	0.63 ± 0.03	5.8 ± 0.9	62 ± 4
CS	–	0.45 ± 0.09	–	–	92 ± 3
CS + BG	31 ± 1	0.50 ± 0.18	0.65 ± 0.02	6.7 ± 0.6	39 ± 5
CS + MIX	38 ± 1	0.54 ± 0.16	0.67 ± 0.07	7.2 ± 1.2	45 ± 6

ZP - zeta potential, D_w - deposit weight, R_a - roughness average, R_{max} - maximum roughness depth, WCA - water contact angle.

3.1.6. ATR-FTIR

Fig. 2a presents FTIR spectra of particles (BG, MBGN) in powder form and coatings (pure CS, CS + BG) deposited on stainless steel (AISI 316L) substrate for 600 s (25 V), shown as a reference for the less intensive FTIR spectra for the coatings deposited on the pre-treated WE43 substrate (Fig. 2b). The main bands obtained for the BG particles (SiO_2-CaO-Na_2O-P_2O_5 system) at ~1000 cm^{-1} and ~915 cm^{-1} can be assigned to Si—O—Si stretching vibrations (Fig. 2a). The dual nature of these bands is due to the presence of network modifiers such as Ca and Na in the glass structure [48], while for MBGN particles (SiO_2-CaO system) this band appears at ~1030 cm^{-1}. For both types of particles, the band at ~450 cm^{-1} can be attributed to Si-O-Si bending vibrations [49]. Additionally, the band at ~1450 cm^{-1} for BG particles can be related to carbonate groups adsorbed from the atmosphere. In the spectrum obtained for the CS coating on AISI 316L substrate, the broad band in the range 3700–3000 cm^{-1} is due to overlapping of several bands, i.e. the stretching vibration of O-H, absorbed water and N—H stretching of amine and amide [42], while the vibration bands of the C—H is at ~2920 cm^{-1} and ~2875 cm^{-1}. Additionally, signals at 1375 cm^{-1} (—CH_3) and 1420 cm^{-1} (—CH_2) are also present [42,50]. The peaks at ~1645, ~1560 and ~1315 cm^{-1} can be assigned to the N—H bending of the amine groups I, II and III respectively [50,51]. Bands at ~1060 and ~1027 cm^{-1} represent the C—O vibrations [42] of the CS and peaks at ~893 and ~1152 cm^{-1} correspond to the saccharide structure of CS [50]. The spectrum obtained for CS + BG coating on AISI 316L substrate consists of characteristic bands of BG and CS, indicating incorporation of both components into the coating. The hydrogen bonding between CS and BG is observed as the reduction of band at 1645 cm^{-1} to band at 1560 cm^{-1} (highlighted on Fig. 2a).

The spectrum obtained for the pre-treated WE43 samples (Fig. 2b) reveals strong bands from carbonate and phosphate groups at ~1405 and ~1007 cm^{-1}, respectively [39]. Interestingly, the intensities of those peaks decrease after the EPD coating process. The spectra obtained on the coated surfaces show bands related to the coating components and to the surface pre-treatment (Fig. 2b). However, due to the limited thickness of the deposited coatings caused by the used deposition parameters, the intensity of peaks is lower than that obtained for the reference samples.

3.1.7. Corrosion studies

Fig. 3a presents typical Nyquist plots of the composite coated samples (CS + BG, CS + MIX) compared to the bare (without pre-treatment) and DMEM pre-treated WE43 substrates obtained after 1 h immersion in 0.1 NaCl. For the bare WE43 substrate, the plot with two capacitive loops (at high and medium frequencies) and an inductive loop (at low frequencies) [52] indicates the impact of formed corrosion products layer on the surface during 1 h immersion in 0.1 NaCl with the polarization resistance (R_p) of ~2 kΩcm^2. As expected from the pretreatment procedure, a significant higher R_p (~7 kΩcm^2) for the pre-treated WE43 substrate proves a thicker barrier on the surface which enhances the corrosion resistance. The values of R_p for the composite coated samples are between the bare and pre-treated WE43 substrates (~5 kΩcm^2), where the CS + MIX sample exhibits a lower R_p than the CS + BG. A more pronounced second capacitive loop (medium frequencies) in Nyquist plots, which represents the resistance and the capacity of the surface layer, indicates the effect of CS + BG and CS + MIX composite coatings [52].

Potentiodynamic polarization curves for the tested samples (Fig. 3b) indicate a reduction of the anodic current densities (shown as plateau up

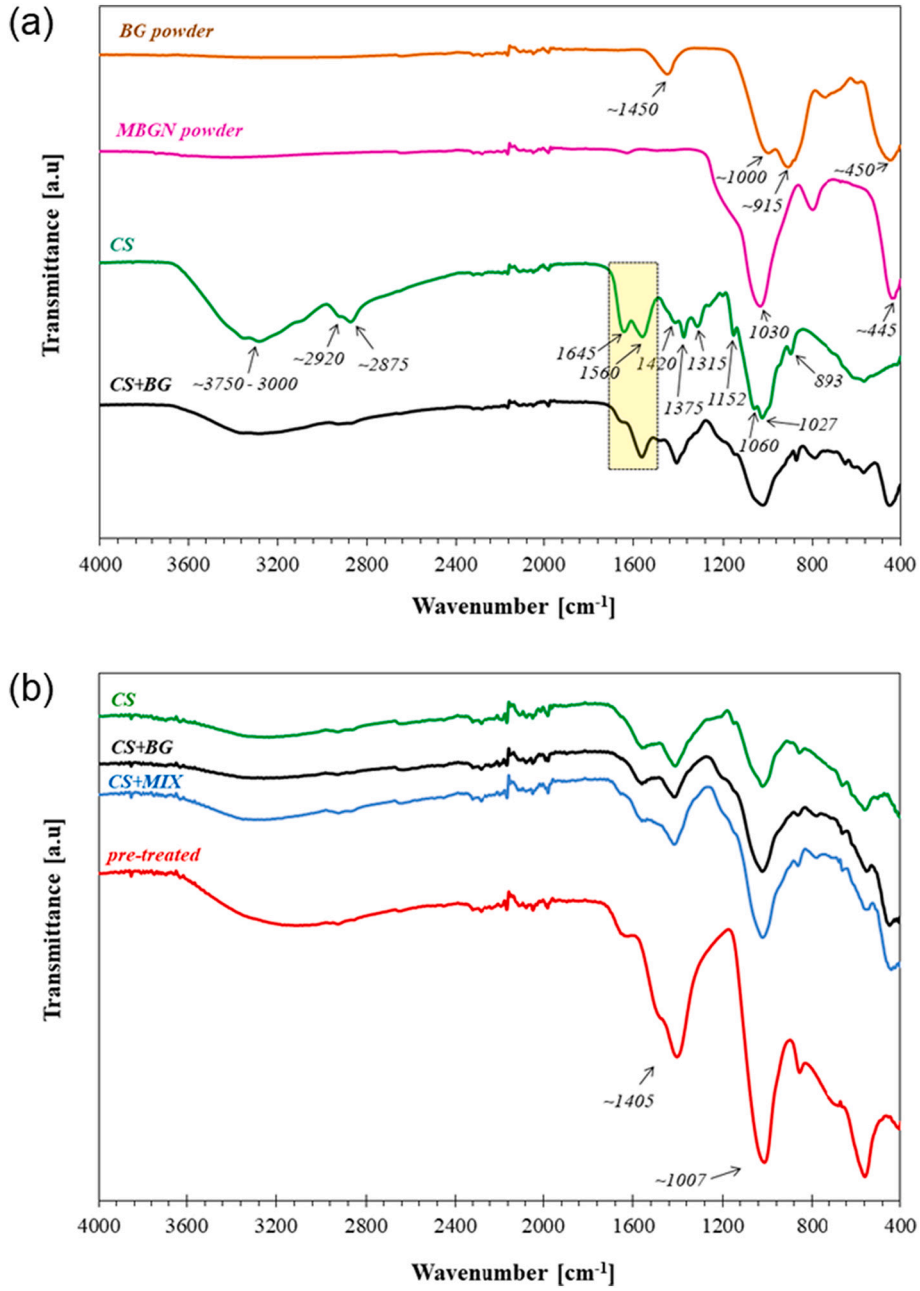

Fig. 2. FTIR spectra for: a) BG and MBGN particles and typical spectra of CS and CS + BG coatings on AISI 316L (600 s, 25 V), b) pre-treated WE43 substrate, coated (pure CS, CS + BG, CS + MIX; 60 s, 50 V) pre-treated WE43 substrate. (The relevant peaks and highlighted area are described in the text.)

to a breakdown potential) for the pre-treated WE43 substrate and composite coated (CS + BG, CS + MIX) samples compared to the bare WE43 substrate. However, the presence of the CS + BG or CS + MIX coating on the pre-treated WE43 substrate slightly increases the anodic current density compared to the pre-treated substrates. The I_{corr} for the bare WE43 is 10.3 μA/cm^2, while for pre-treated WE43, CS + BG and CS + MIX the I_{corr} is 3.9 μA/cm^2, 6.6 μA/cm^2 and 7.2 μA/cm^2, respectively. Both, the Nyquist plots and potentiodynamic polarization curves, demonstrate the positive impact of the applied surface modification on the improvement of corrosion resistance of the bare WE43 substrate. Between CS + BG and CS + MIX coatings only a slight difference can be observed.

3.2. Cell study

3.2.1. Cell metabolic activity

Fig. 4 shows differences in the reduction of alamarBlue® by ST-2 cells on the reference (pre-treated, pure CS-coated) and the composite (CS + BG, CS + MIX) coated samples. The higher the value of the reduction, which is associated with higher cell metabolic activity, the higher the ST-2 cell proliferation. The trend for 2 d shows that cell proliferation was higher for the pre-treated sample followed by the composite (CS + MIX, CS + BG) coated and the CS coated samples, however, a significant difference ($p < 0.05$) was found only between the pre-treated and pure CS samples. For 7 d the trend becomes: CS + MIX > pre-treated > CS + BG > CS; however, significant differences ($p < 0.05$) were found between pure CS/pre-treated, CS + MIX/pure CS and CS + MIX/CS + BG samples.

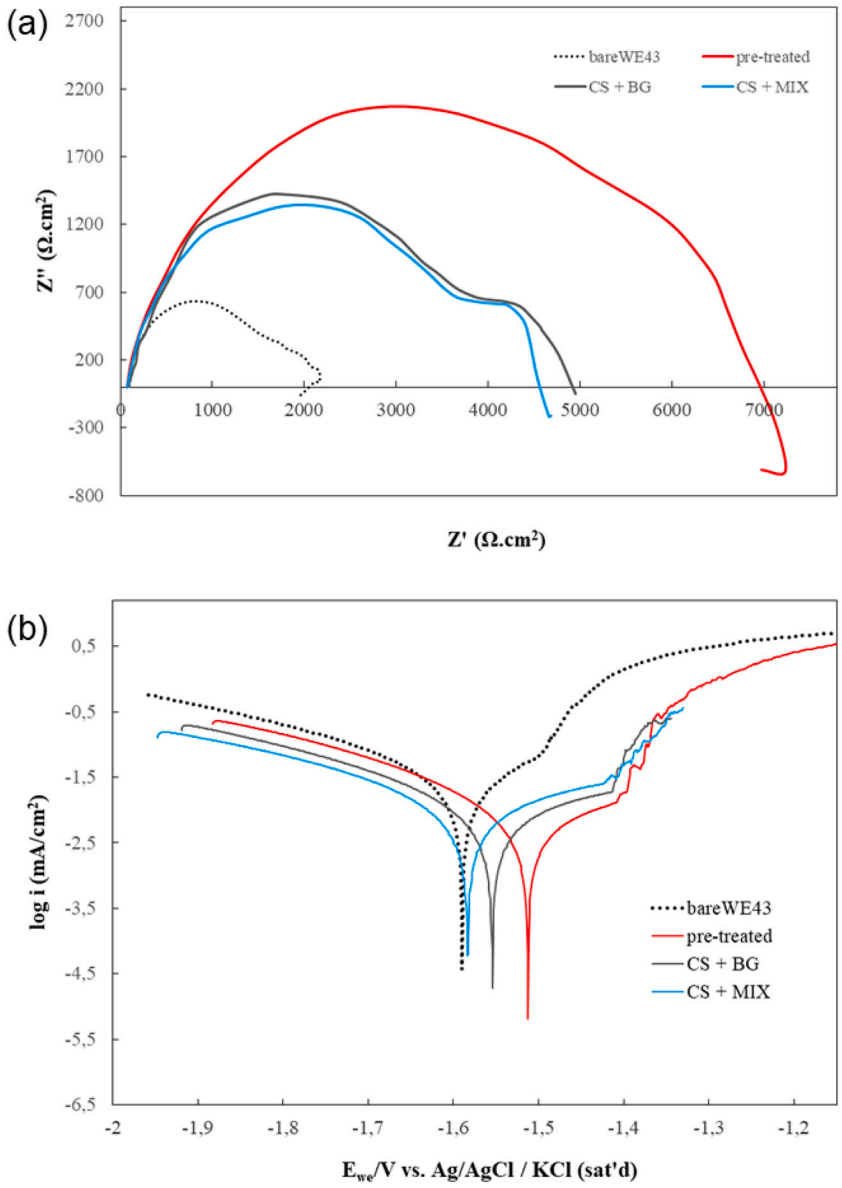

Fig. 3. Corrosion study of the composite (CS + BG and CS + MIX) coated and pre-treated WE43 substrates, the bare and pre-treated WE43 substrates after immersion in 0.1 NaCl for 1 h; a) Nyquist plots, b) potentiodynamic polarization curves.

3.2.2. Cell functionalization

Fig. 5a shows the total protein concentration for the references (pre-treated, pure CS coated) and composite coated (CS + BG, CS + MIX) samples, which can be correlated to the viable cells. The total protein concentration differs among the samples. After 7 d, the trend can be summarized as CS + MIX > pre-treated > CS, CS + BG, while significant differences ($p < 0.05$) were found between CS + MIX and pure CS and between CS + MIX and CS + BG samples. For 10 d, the trend becomes: pre-treated > CS + BG, CS + MIX > CS, however no significant difference was found between samples. The relative ALP activity also differs between tested samples and decreases with time for all of them, including the positive control (+) (Fig. 5b). For 7 d, the relative ALP activity trend can be summarized as CS ≫ CS + MIX > CS + BG > pre-treated. The significant difference was found between pure CS and the other samples. After 10 d this trend becomes: CS + BG > CS > CS + MIX, pre-treated, however no significant difference was found between samples.

3.2.3. pH changes and weight loss

Fig. 6a shows the pH of the osteogenic media at 7 d and 10 d. The presence of the samples in the osteogenic medium with ST-2 cells significantly ($p < 0.001$) increases the pH from 7.65 [(+) and (−) controls] to ~8.00–8.20. The values of pH for coated (pure CS, CS + BG, CS + MIX) samples are slightly higher than for the pre-treated, whereas the pH for pure CS-coated sample is the highest among samples ($p < 0.05$). The W_{loss} differs between sample types and increases in time for all of them (Fig. 6b). At 7 d, the W_{loss} for the pre-treated sample is ~8.5 ± 0.4 μg/mm^2, while for pure CS, CS + BG and CS + MIX the W_{loss} is ~12.4 ± 2.2 μg/mm^2, ~10 ± 1.9 μg/mm^2 and ~11 ± 0.7 μg/mm^2, respectively. At 10 d, the W_{loss} for the pre-treated sample is ~8.9 ± 1.2 μg/mm^2, while for pure CS, CS + BG and CS + MIX it is ~20.4 ± 4.4 μg/mm^2, ~13 ± 1.2 μg/mm^2 and ~ 13.6 ± 1.5 μg/mm^2, respectively. A general trend for the W_{loss} can be summarized as: CS ≫ CS + MIX > CS + BG > pre-treated. However, significant differences ($p < 0.05$) were found between pure CS and pre-treated and between pure CS and CS + BG samples at 10 d and between pure CS and the other samples ($p < 0.001$) at 16 d.

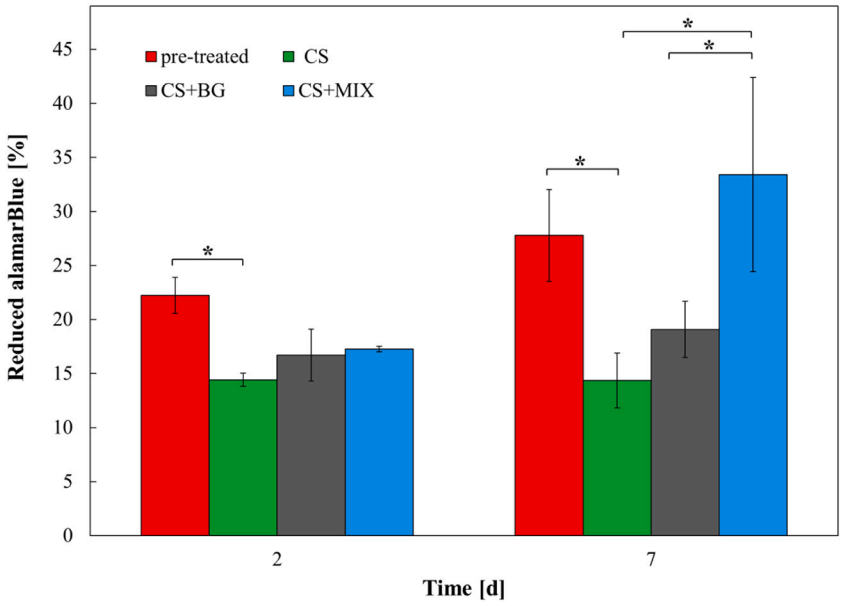

Fig. 4. Reduced alamarBlue® amount of ST-2 cells on pre-treated and coated (pure CS, CS + BG, CS + MIX) WE43 samples after 2 and 7 d of incubation (mean ± S. D., n = 4). Statistically significant differences are highlighted (*$p < 0.05$) between samples at the same time points.

3.2.4. Surface observations

Fig. 7a–b present the initial microstructure of WE43 sample, consisting of equiaxed grains (~15 μm) with α-Mg rich regions and randomly dispersed second phase precipitations [49]. Surface morphologies after cell functionality examination and chromic acid cleaning differ among samples (Fig. 7c–f). The specific "grain boundaries" pattern is visible on every type of sample, however its intensity and depth vary between samples. On the pre-treated surface some residues of the initial surface, indicating the pattern of polishing direction, are still visible (Fig. 7c), while previously coated surfaces (pure CS, CS + BG, CS + MIX) are rougher with localized corrosion in α-Mg rich regions. Localized corrosion (shown as pits on the surface) increased in time for all type of samples by pits deepening (Fig. 8) pointing to the previously CS-coated surfaces as being the most affected (Fig. 8b, f).

4. Discussion

4.1. Medium and high M_w composite coatings (CS + BG)

The quality of the functional coating on Mg-based implants plays a crucial role in its final performance. Heise et al. [29] found that for CS with medium M_w (190–310 kDa) and DDA (75–85%) the best quality of electrophoretic CS + BG composite coating on pre-treated WE43 substrates was achieved at 50 V and 120 s deposition time.

This study reveals that for CS with high M_w (340–360 kDa) and DDA (≥95%), the best quality of CS + BG composite coatings in terms of continuity and homogeneity was obtained by EPD at 50 V and 60 s (Fig. 1c–d). Despite shorter deposition time than in case of medium M_w CS-based composite coating [29], the achieved CS + BG coating also improved the corrosion resistance of bare WE43 substrate (Fig. 3a–b). An increase of the deposition time caused formation of coating defects such as discontinuities related to entrapped gas bubbles (see Supplementary data Figs. S1–2). Presumably, this effect is related to a denser packing of CS molecules on the surface when high M_w CS was used in comparison to medium M_w. The use of CS with higher M_w and DDA corresponds to higher levels of available protonated amine-groups in the EPD suspension. Additionally, a higher DDA gives fewer large acetyl side groups in CS resulting in a more regular packing of the chains in the polymer structure and in a less amorphous structure. Therefore, the H_2 which accompanies EPD of CS-based coatings on Mg-based substrates (Eqs. (1) and (3)) may be entrapped in form of gas bubbles much faster by the deposited CS coating. This leads to the conclusion that CS characteristics may influence the deposition time of CS + BG coatings fabricated via EPD.

4.2. M_w CS-based composite coatings

In this study, the CS + BG and CS + MIX composite coatings based on CS with high M_w (340–360 kDa) with DDA (≥95%) and bioactive particles (BG, MBGN) with different sizes (micro, nano), morphologies (solid, mesoporous), shapes (non-spherical, spherical), chemical compositions (SiO_2-CaO-Na_2O-P_2O_5 and SiO_2-CaO systems) and fabrication method (melt-derived, sol-gel) were deposited on pre-treated WE43 substrates via EPD. The optimized parameters (50 V, 60 s) resulted in continuous coatings with homogeneously distributed BG particles in both composites (Fig. 1c–f). The partial replacement of micron size BG with nano size MBGN particles additionally caused filled spaces between BG particles or assembled single MBGN particles and their agglomerates, even larger than 2 μm (marked by arrows in Fig. 1g–h) on top of the BG particles. For both coatings no delamination from the pre-treated substrates was observed following a tape test similar to the one carried out in a previous study [29]. Despite the equal organic/inorganic components weight ratio (1:2) in both suspensions, the deposit weight [$D_w = (W_d - W_{initial}) / S_o$] for the CS + MIX coating was slightly higher (Table 1) than for the CS + BG coating. This difference can be related to the BG/MBGN weight ratio (3:1) and/or different particles sizes [22]. However, both factors can influence the particle mobility during EPD and consequently also the contribution of the particles and molecules to the composite. ZP values are slightly higher for the mixture of particles (CS + MIX) than for one type of particles (CS + BG) (Table 1). Pure BG particles have negative ZP while CS molecules are positively charged at the used pH. Change of the particles ZP from negative to positive proves formation of particle-polymer complexes enabling cathodic deposition via EPD [43]. FTIR data confirmed the bonding between CS molecules and particles (marked on Fig. 2a). Presumably, a larger specific surface area of MBGN (spherical, nano, mesoporous) [33] than BG (non-spherical, micro, solid) particles may also have an impact on achieving a better interaction with the CS matrix. However, the Nyquist plots indicate marginal impact of the type of used particles (micro sized for the CS + BG or mixture of micro and nano sized for the CS + MIX) on the R_p for

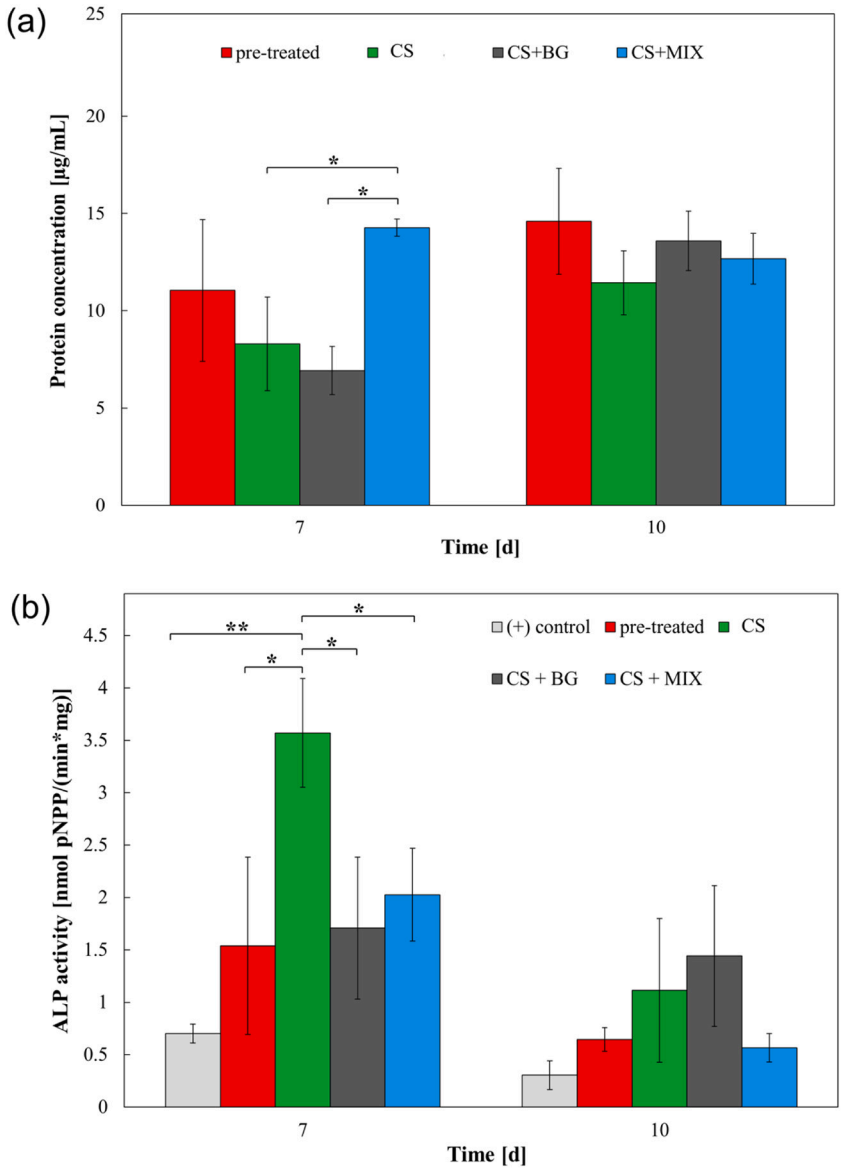

Fig. 5. Data obtained for ST-2 cell line on pre-treated and coated (pure CS, CS + BG, CS + MIX) WE43 samples at different time points (7 d and 10 d), a) normalized total protein concentration (mean ± s.d., n = 3); b) normalized ALP activity, (mean ± s.d., n = 3). Statistically significant differences are highlighted (*$p < 0.05$, **$p < 0.001$) between samples at the same time points.

the composite coatings (Fig. 3a), whereas a slightly higher current density and I_{corr} were noticed for CS + MIX than CS + BG (Fig. 3b).

Bioactive glass particles, beside the high potential in the bioactivity improvement by introducing HA nucleation sites, induce a surface topography to the pre-treated WE43 substrate [29] and increase its surface roughness (Table 1). This effect is more prominent for CS + MIX than CS + BG coating. Additionally, the superficial silanol-groups (Si-OH) of particles [53] are responsible for a higher wettability of the composite-coated than the pure CS-coated or the pre-treated samples (Table 1). However, the slightly higher WCA for CS + MIX coating (45° ± 6) than for CS + BG coating (39° ± 5) can be related to the coating topography and/or higher adsorption of the CS molecules on MBGN particles. It has been reported that a WCA between 35° and 80° is beneficial for bone cell attachment [54]. However, some studies have reported that WCA of ~70° is favorable for cell proliferation [55], while others consider 55° as the optimum [56]. The cell study performed on samples revealed differences in ST-2 cell response (Fig. 4). For the coated samples, addition of the particles to the CS matrix improved the cell response at 7 d. This effect was significantly higher ($p < 0.05$) for CS + MIX coating than for CS + BG coating. The trend for the total protein concentration at 7 d seems to support this finding (Fig. 5a). Additionally, the protein increases over time (Fig. 5a), confirming cell continuous proliferation and simultaneous decrease of the relative ALP activity, may suggest a progress of mineralization on the surface (Fig. 5b). This progress is utmost for the CS + MIX sample, while for pure CS sample it can be affected by substrate corrosion. Mg ions in certain amounts can activate and stimulate ALP activity giving false results due to chellating with Mg ions. This effect increases with Mg ion concentration [57,58], hence it is crucial to monitor the samples' ALP activity and the W_{loss}.

4.3. Corrosion sensitivity and cellular response: pre-treated vs coated samples

DMEM pre-treatment was applied [29,39] to suppress the corrosion of the bare WE43 substrate, in order to enable the fabrication of composite coatings (CS + BG, CS + MIX) via EPD. DMEM pre-treatment performed on pure Mg substrate results in the formation of a temporary barrier (~3.5 µm thickness) on its surface [39]. This temporary

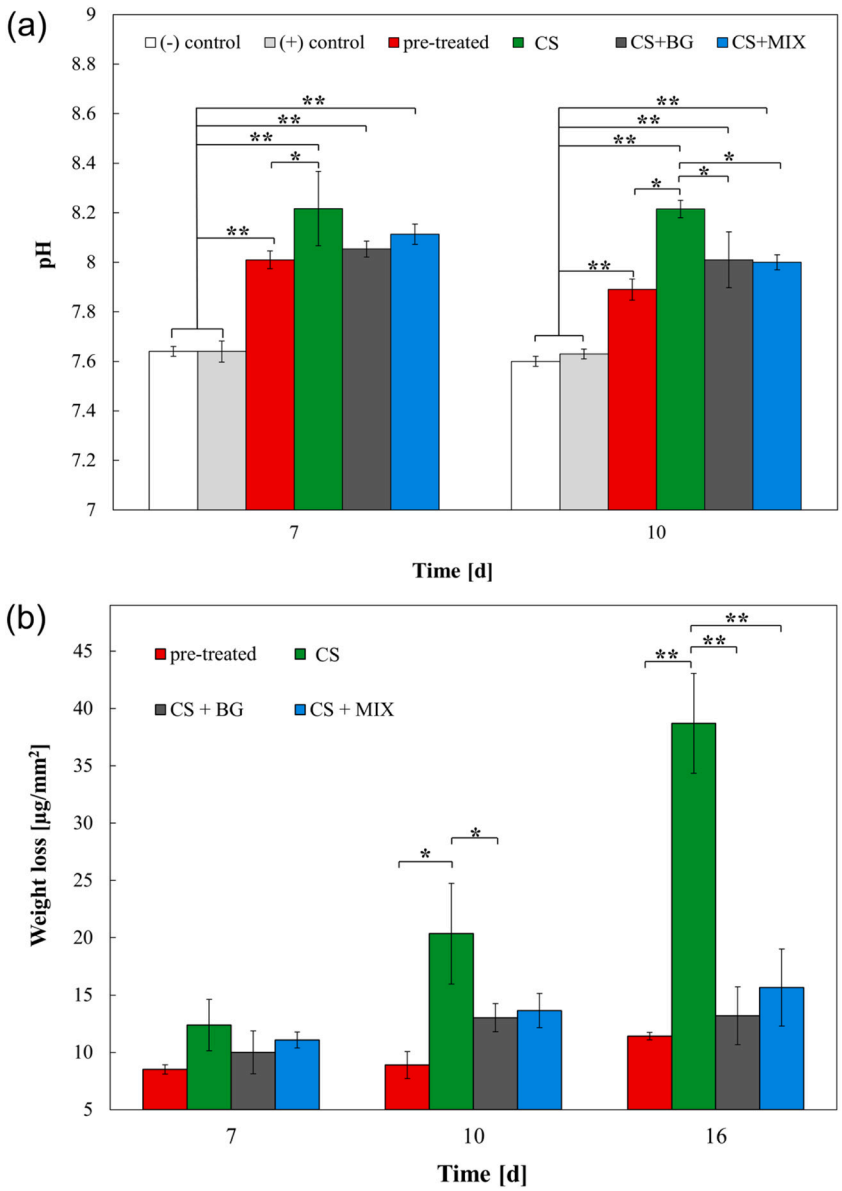

Fig. 6. a) pH of osteogenic differentiation medium at 7 d and 10 d (mean ± s.d., n = 3); b) W_{loss} for references (pre-treated WE43, pure CS coating) and composite (CS + BG, CS + MIX) coated samples incubated with ST-2 cell line and cleaned in chromic acid solution (mean ± s.d., n = 3). Statistically significant differences are highlighted (*p < 0.05, **p < 0.001) between samples at the same time points.

barrier has a significant impact on the substrate's initial corrosion suppression, fabrication of the composite coatings or cell response. In this study, FTIR measurements on the DMEM pre-treated WE43 substrate show the presence of signals related to phosphate and carbonate groups (Fig. 2b) similar to the ones obtained for pure Mg substrates [39]. For coated samples those signals are reduced or suppressed by those from the coatings components. A proper evaluation of any functional composite coating on Mg-based implants requires both cell response and long-term corrosion evaluation, preferably in in vitro conditions as both factors have a mutual influence.

The cell study performed on the pre-treated and coated (pure CS, CS + BG, CS + MIX) samples revealed differences in ST-2 cell response after 2 d, indicating the pre-treated sample as the most beneficial for cell metabolic activity, while CS + MIX sample gains comparable positive effects after 7 d (no significant difference) (Fig. 4). Other coated samples (pure CS and CS + BG) show significant lower impact on the cells comparable to CS + MIX. The beneficial effect of the pre-treated samples can be linked to the presence of a temporary barrier and the composition of the pre-treatment solution (DMEM), being a cell culture medium used to grow and feed cells. DMEM contains components such as inorganic salts, amino acid, vitamins, which during the pre-treatment procedure were incorporated as a temporary barrier and can explain the positive response of the cells in contact with the pre-treated surface. Furthermore, these samples were not immersed in the acidic CS-based solution or subjected to conditions simulating the EPD process, thus the comparison is not fully justified. Indeed, the mentioned procedures could strongly influence the stability of the temporary barrier created during the pre-treatment. However, it must be mentioned that DMEM pre-treatment alone does not secure surface bioactivity, while the optimization of the coating components does. Both, pure CS (no particles) and CS + BG (micro size particles) samples showed less positive effect on cell proliferation and functionalization than DMEM pre-treatment, while the CS + MIX (mixture of micro and nano particles) exhibited a positive effect. Nyquist plots showed lower R_p values for the composite coated pre-treated samples than for the pre-treated only sample but they were higher than for bare WE43, while potentiodynamic curves confirmed the

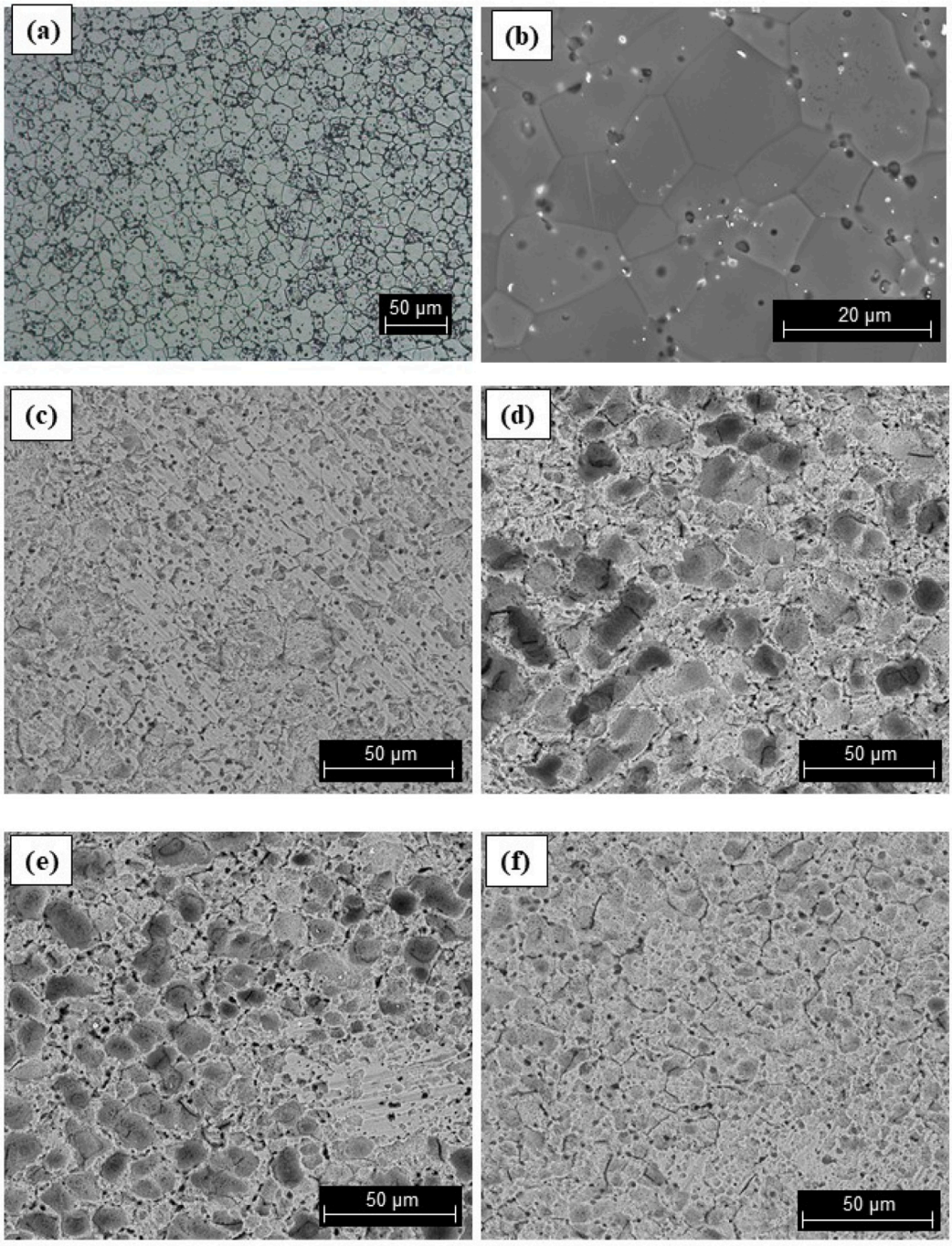

Fig. 7. (a–b) microstructure of initial WE43 substrate (optical and SEM image, respectively), (c–f) SEM images of surface morphology after 7 d of ALP experiment and chromic acid cleaning for the pre-treated WE43 substrate, pure CS, CS + BG, CS + MIX, respectively.

lowest current density and I_{corr} for the pre-treated sample (Fig. 3a–b). Long-term incubation in *in vitro* conditions (cell functionalization study) revealed slightly higher pH of the osteogenic medium for the coated samples than for the pre-treated samples, although a significant difference ($p < 0.05$) was found only between pure CS and the pre-treated samples (7 d) or between pure CS and the other samples (10 d) (Fig. 6a). High pH may be associated to (i) dissolution of the embedded particles (BG, MBGN) during HA formation [59,60] and (ii) substrate corrosion. However, the highest pH for the pure CS-coated samples suggests that the EPD process plays a dominant role in the final substrate corrosion sensitivity. Presumably, the stability of the temporary barrier created by the DMEM pretreatment decreases during EPD for all coated samples. However, during the cell culture study particles embedded in the CS matrix (CS + BG and CS + MIX samples) suppress this negative impact by the formation of HA on the surface (see Supplementary data, Figs. S3–4). However, more research is needed to prove this hypothesis. Nevertheless, the pH trend correlates with the trend of the samples W_{loss} (CS ≫ CS + MIX > CS + BG > pre-treated) (Fig. 6b). Additionally, surface morphologies after cleaning vary between samples, indicating the pre-treated one as the least affected by localized corrosion (Fig. 7c–f). The specific "grain boundaries" pattern is more obvious on the previously coated samples. However, the pure CS-coated sample was found to be the most corroded one after 16 d (Fig. 8).

The obtained results suggest that the CS + MIX coating is a promising

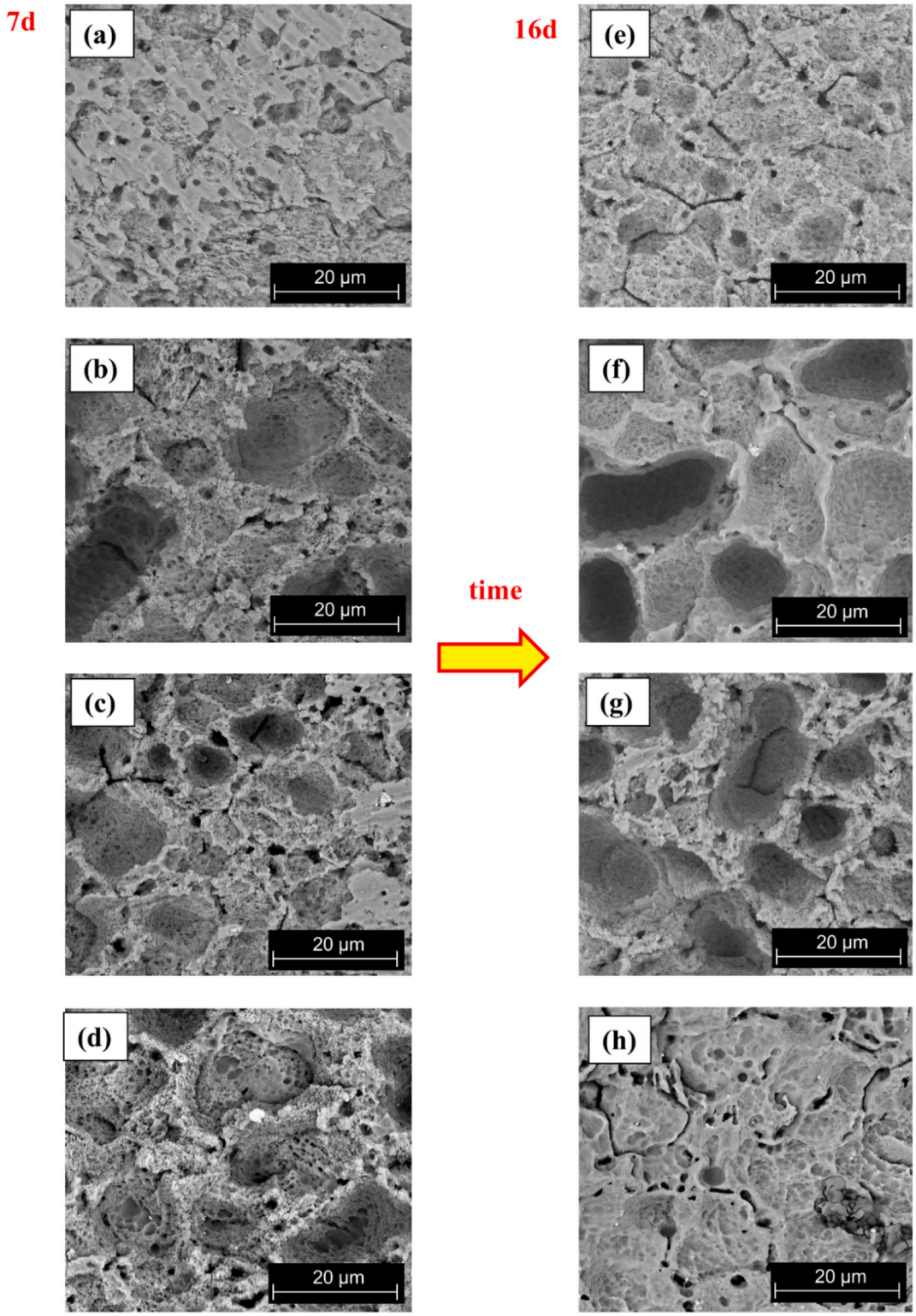

Fig. 8. Higher magnification SEM images of the surface morphology after ALP experiment and chromic acid cleaning: (a, e) pre-treated WE43 substrate, (b, f) pure CS, (c, g) CS + BG, (d, h) CS + MIX for 7 d (a–d) and 16 d (e–h), respectively.

functional composite coating for Mg-based implants, because it ensures control of substrate degradation and positive cell response up to 16 d. However, further investigations, potentially *in vivo* studies, are needed for further characterization of the pre-treated and CS + MIX coated samples.

5. Conclusions

This study presented the electrophoretic deposition of homogeneous composite coatings based on high M_w CS (M_w 340–360 kDa, DDA $\geq$ 95%) and embedded bioactive glass particles: solid micron sized BG (CS + BG coating) and a mixture of micrometric BG with mesoporous nano sized MBGN (CS + MIX coating) on Mg-based substrates. The presence of

the composite coatings on the pre-treated WE43 substrate influenced surface topography, wetting properties, corrosion resistance and cell response, indicating that the CS + MIX coating is more beneficial than CS + BG in terms of cell response (proliferation and functionalization).

It was found that different M_W (and DDA) of CS used as the matrix for BG particles may influence the deposition time needed for homogeneous electrophoretic composite coatings on pre-treated WE43 substrates. This is important for the decrease of deposition time, thus minimizing the negative impact of acidic CS-based solutions and applied EPD conditions on the Mg-based substrate corrosion sensitivity. However, CS characteristics may also influence coating properties such as thickness or biodegradation, which are crucial for the applications of Mg-based implant. Thus, a more detailed study on the long-term behavior of CS-based composite coatings, both *in vitro* and *in vivo*, is needed.

Obtained data suggest that the fabrication conditions of CS-based coatings on pre-treated WE43 substrates via EPD may adversely affect the substrate corrosion sensitivity. However, despite the slightly higher corrosion sensitivity of the WE43 substrates with CS + MIX coating in comparison to pre-treated WE43 substrates, the coated sample gains comparable positive effects on the cell proliferation and functionalization. DMEM pretreatment has a positive impact on corrosion resistance of WE43 substrates and on their cell response, however it does not secure bioactive properties or the ability to load antibacterial agents. This is an advantage of the composite coating developed here and thus further research in such CS + MIX system for Mg alloys are justified.

CRediT authorship contribution statement

Agnieszka Witecka: Conceptualization, Methodology, Investigation, Validation, Funding acquisition, Writing – original draft, Writing – review & editing. **Svenja Valet:** Methodology, Writing – review & editing, Supervision. **Michał Basista:** Conceptualization, Writing – review & editing, Funding acquisition. **Aldo Roberto Boccaccini:** Conceptualization, Writing – review & editing, Resources, Supervision.

Declaration of competing interest

The authors declare that they have no known competing financial interests or personal relationships that could have appeared to influence the work reported in this paper.

Acknowledgments

The first author is grateful for the financial support of National Science Centre (Poland) within Miniatura 1 (grant no. DEC-2017/01/X/ST8/00509) and a KMM-VIN Research Fellowship (2018) from the European Virtual Institute on Knowledge-based Multifunctional Materials (KMM-VIN AISBL). The authors would like to thank F. Ruther (FAU) for help with roughness measurements, Dr. K. Zheng (FAU) for providing the MBGN particles, Dr. L. Liverani (FAU) for providing high M_W chitosan and Faculty of Materials Science and Engineering (Warsaw University of Technology, Poland) for the access to their facilities.

Appendix A. Supplementary data

Supplementary data to this article can be found online at https://doi.org/10.1016/j.surfcoat.2021.127232.

References

[1] F. Witte, The history of biodegradable magnesium implants: a review, Acta Biomater. 6 (2010) 1680–1692, https://doi.org/10.1016/j.actbio.2010.02.028.
[2] J.L. Wang, J.K. Xu, C. Hopkins, D.H.K. Chow, L. Qin, Biodegradable magnesium-based implants in orthopedics—a general review and perspectives, Adv. Sci. 7 (2020), 1902443, https://doi.org/10.1002/advs.201902443.
[3] M.E. Maguire, J.A. Cowan, Magnesium chemistry and biochemistry, BioMetals 15 (2002) 203–210, https://doi.org/10.1023/a:1016058229972.
[4] M.P. Staiger, A.M. Pietak, J. Huadmai, G. Dias, Magnesium and its alloys as orthopedic biomaterials: a review, Biomaterials 27 (2006) 1728–1734, https://doi.org/10.1016/j.biomaterials.2005.10.003.
[5] L. Xu, G. Yu, E. Zhang, F. Pan, K. Yang, In vivo corrosion behavior of Mg-Mn-Zn alloy for bone implant application, J. Biomed. Mater. Res. A 83 (2007) 703–711, https://doi.org/10.1002/jbm.a.31273.
[6] S. Dobatkin, N. Martynenko, N. Anisimova, M. Kiselevskiy, D. Prosvirnin, V. Terentiev, N. Yurchenko, G. Salishchev, Y. Estrin, Biodegradation, and biocompatibility of ultrafine grained magnesium alloy WE43, Materials 12 (2019), 3627, https://doi.org/10.3390/ma12213627.
[7] F. Witte, V. Kaese, H. Haferkamp, E. Switzer, A. Meyer-Lindenberg, C.J. Wirth, H. Windhagen, In vivo corrosion of four magnesium alloys and the associated bone response, Biomaterials 26 (2005) 3557–3563, https://doi.org/10.1016/j.biomaterials.2004.09.049.
[8] J. Vormann, Magnesium: nutrition and metabolism, Mol. Asp. Med. 24 (2003) 27–37, https://doi.org/10.1016/S0098-2997(02)00089-4.
[9] K. Kuśnierczyk, M. Basista, Recent advances in research on magnesium alloys and magnesium-calcium phosphate composites as biodegradable implant materials, J. Biomater. Appl. 31 (2017) 878–900, https://doi.org/10.1177/0885328216657271.
[10] A. Witecka, A. Yamamoto, W. Święszkowski, Influence of SaOS-2 cells on corrosion behavior of cast Mg-2.0Zn0.98Mn magnesium alloy, Colloids Surf. B 150 (2017) 288–296, https://doi.org/10.1016/j.colsurfb.2016.10.041.
[11] A. Yamamoto, S. Hiromoto, Effect of inorganic salts, amino acids and proteins on the degradation of pure magnesium in vitro, Mater. Sci. Eng. C 29 (2009) 1559–1568, https://doi.org/10.1016/j.msec.2008.12.015.
[12] A. Witecka, A. Bogucka, A. Yamamoto, K. Máthis, T. Krajňák, J. Jaroszewicz, W. Święszkowski, In vitro degradation of ZM21 magnesium alloy in simulated body fluids, Mater. Sci. Eng. C 65 (2016) 59–69, https://doi.org/10.1016/j.msec.2016.04.019.
[13] F. Witte, N. Hort, C. Vogt, S. Cohen, K.U. Kainer, R. Willumeit, F. Feyerabend, Degradable biomaterials based on magnesium corrosion, Curr. Opin. Solid State Mater. Sci. 12 (2008) 63–72, https://doi.org/10.1016/j.cossms.2009.04.001.
[14] G.L. Song, A. Atrens, Corrosion mechanisms of magnesium alloys, Adv. Eng. Mater. 1 (1999) 11–33, https://doi.org/10.1002/(SICI)1527-2648(199909)1:1<11::AIDADEM11>3.0.CO;2-N.
[15] R.B. Heimann, Magnesium alloys for biomedical applications: advanced corrosion control through surface coating, Surf. Coat. Technol. 405 (2021), 126521, https://doi.org/10.1016/j.surfcoat.2020.126521.
[16] A. Witecka, A. Yamamoto, H. Dybiec, W. Swieszkowski, Surface characterization and cytocompatibility evaluation of silanized magnesium alloy AZ91 for biomedical applications, Sci. Technol. Adv. Mater. 13 (2012), https://doi.org/10.1088/1468-6996/13/6/064214.
[17] J.N. Oliver, Y. Su, X. Lu, P.H. Kuo, J. Du, D. Zhu, Bioactive glass coatings on metallic implants for biomedical applications, Bioact. Mater. 4 (2019) 261–270, https://doi.org/10.1016/j.bioactmat.2019.09.002.
[18] L. Xu, A. Yamamoto, Characteristics and cytocompatibility of biodegradable polymer film on magnesium by spin coating, Colloids Surf. B 93 (2012) 67–74, https://doi.org/10.1016/j.colsurfb.2011.12.009.
[19] A. Witecka, A. Yamamoto, J. Idaszek, A. Chlanda, W. Świeszkowski, Influence of biodegradable polymer coatings on corrosion, cytocompatibility and cell functionality of Mg-2.0Zn-0.98Mn magnesium alloy, Colloids Surf. B 144 (2016) 284–292, https://doi.org/10.1016/j.colsurfb.2016.04.021.
[20] A. Akbar, A. Shakeel, A review on chitosan and its nanocomposites in drug delivery, Int. J. Biol. Macromol. 109 (2018) 273–286, https://doi.org/10.1016/j.ijbiomac.2017.12.078.
[21] P. Roach, D. Eglin, K. Rohde, Modern biomaterials: a review-bulk properties and implications of surface modifications, J. Mater. Sci. Mater. Med. 18 (2007) 1263–1277, https://doi.org/10.1007/s10856-006-0064-3.
[22] L. Besra, M. Liu, A review on fundamentals and applications of electrophoretic deposition (EPD), Prog. Mater. Sci. 52 (2007) 1–61, https://doi.org/10.1016/j.pmatsci.2006.07.001.
[23] A.R. Boccaccini, S. Keim, R. Ma, Y. Li, I. Zhitomirsky, Electrophoretic deposition of biomaterials, J. R. Soc. Interface 7 (2010) S581–S613, https://doi.org/10.1098/rsif.2010.0156.focus.
[24] S. Seuss, A.R. Boccaccini, Electrophoretic deposition of biological macromolecules, drugs, and cells, Biomacromolecules 14 (2013) 3355–3369, https://doi.org/10.1021/bm401021b.
[25] E. Avcu, F.E. Baştan, H.Z. Abdullah, M.A.U. Rehman, Y.Y. Avcu, A.R. Boccaccini, Electrophoretic deposition of chitosan-based composite coatings for biomedical applications: a review, Prog. Mater. Sci. 103 (2019) 69–108, https://doi.org/10.1016/j.pmatsci.2019.01.001.
[26] R. Sikkema, K. Baker, I. Zhitomirsky, Electrophoretic deposition of polymers and proteins for biomedical applications, Adv. Colloid Interf. Sci. 284 (2020), 102272, https://doi.org/10.1016/j.cis.2020.102272.
[27] F. Ordikhani, A. Simchi, Long-term antibiotic delivery by chitosan-based composite coatings with bone regenerative potential, Appl. Surf. Sci. 317 (2014) 56–66, https://doi.org/10.1016/j.apsusc.2014.07.197.
[28] S. Heise, T. Wirth, M. Höhlinger, Y.T. Hernández, J.A.R. Ortiz, V. Wagener, S. Virtanen, A.R. Boccaccini, Electrophoretic deposition of chitosan/bioactive glass/silica coatings on stainless steel and WE43 Mg alloy substrates, Surf. Coat. Technol. 344 (2018) 553–563, https://doi.org/10.1016/j.surfcoat.2018.03.050.
[29] S. Heise, M. Höhlinger, Y.T. Hernández, J.J.P. Palacio, J.A. Rodriquez Ortiz, V. Wagener, S. Virtanen, A.R. Boccaccini, Electrophoretic deposition and characterization of chitosan/bioactive glass composite coatings on Mg alloy

substrates, Electrochim. Acta 232 (2017) 456–464, https://doi.org/10.1016/j.electacta.2017.02.081.
[30] L.L. Hench, Bioceramics, J. Am. Ceram. Soc. 81 (1998) 1705–1728, https://doi.org/10.1111/j.1151-2916.1998.tb02540.x.
[31] A. Hoppe, N. Guldal, A.R. Boccaccini, A review of the biological response to ionic dissolution products from bioactive glasses and glass-ceramics, Biomaterials 32 (2011) 2757–2774, https://doi.org/10.1016/j.biomaterials.2011.01.004.
[32] K. Zheng, A.R. Boccaccini, Sol-gel processing of bioactive glass nanoparticles: a review, Adv. Colloid Interf. Sci. 249 (2017) 363–373, https://doi.org/10.1016/j.cis.2017.03.008.
[33] K. Zheng, E. Torre, A. Bari, N. Taccardi, C. Cassinelli, M. Morra, S. Fiorilli, G. Iviglia Ch. Vitale-Brovarone, A.R. Boccaccini, Antioxidant mesoporous Ce-doped bioactive glass nanoparticles with anti-inflammatory and pro-osteogenic activities, Materials Today Bio 5 (2020), 100041, https://doi.org/10.1016/j.mtbio.2020.100041.
[34] F. Croisier, C. Jérôme, Chitosan-based biomaterials for tissue engineering, Eur. Polym. J. 49 (2013) 780–792, https://doi.org/10.1016/j.eurpolymj.2012.12.009.
[35] H. Zhang, S.H. Neau, In vitro degradation of chitosan by a commecial enzyme preparation: effect of molecular weight and degree of deacetylation, Biomaterials 22 (2000) 1653–1658, https://doi.org/10.1016/S0142-9612(00)00326-4.
[36] S.H. Pangburn, P.V. Trescony, J. Heller, Lysozyme degradation of partially deacetylated chitin, its films and hydrogels, Biomaterials 3 (1982) 105–108, https://doi.org/10.1016/0142-9612(82)90043-6.
[37] M. Rinaudo, Chitin and chitosan: properties and applications, Prog. Polym. Sci. 31 (2006) 603–632, https://doi.org/10.1016/B978-0-12-817970-3.00001-8.
[38] I. Zhitomirsky, Cathodic electrodeposition of ceramic and organoceramic materials. Fundamental aspects, Adv. Colloid Interf. Sci. 97 (2002) 279–317, https://doi.org/10.1016/s0001-8686(01)00068-9.
[39] V. Wagener, S. Virtanen, Protective layer formation on magnesium in cell culture medium, Mater. Sci. Eng. C 63 (2016) 341–351, https://doi.org/10.1016/j.msec.2016.03.003.
[40] M. Höhlinger, S. Heise, V. Wagener, A.R. Boccaccini, S. Virtanen, Developing surface pre-treatments for electrophoretic deposition of biofunctional chitosan-bioactive glass coatings on a WE43 magnesium alloy, Appl. Surf. Sci. 405 (2017) 441–448, https://doi.org/10.1016/j.apsusc.2017.02.049.
[41] S. Clavijo, F. Membrives, G. Quiroga, A.R. Boccaccini, M.J. Santillan, Electrophoretic deposition of chitosan/Bioglass® and chitosan/Bioglass®/TiO_2 composite coatings for bioimplants, Ceram. Int. 42 (2016) 14206–14213, https://doi.org/10.1016/j.ceramint.2016.05.178.
[42] F. Pishbin, V. Mourino, G.J. B., D.W. McComb, S. Kreppel, V. Salih, M.P. Ryan, A. R. Boccaccini, Single-step electrochemical deposition of antimicrobial orthopaedic coatings based on a bioactive glass/chitosan/nano-silver composite system, Acta Biomater. 9 (2013) 7469–7479, https://doi.org/10.1016/j.actbio.2013.03.006.
[43] F. Pishbin, A. Simchi, M.P. Ryan, A.R. Boccaccini, Electrophoretic deposition of chitosan/45S5 Bioglass® composite coatings for orthopaedic applications, Surf. Coat. Technol. 205 (2011) 5260–5268, https://doi.org/10.1016/j.surfcoat.2011.05.026.
[44] F. Ordikhani, S. Petrova Zustiak, A. Simchi, Surface modifications of titanium implants by multilayer bioactive coatings with drug delivery potential: antimicrobial, biological, and drug release studies, JOM 68 (2016) 1100–1108, https://doi.org/10.1007/s11837-016-1840-2.
[45] D. Zhitomirsky, J.A. Roether, A.R. Boccaccini, I. Zhitomirsky, Electrophoretic deposition of bioactive glass/polymer composite coatings with and without HA nanoparticles inclusions for biomedical applications, J. Mater. Process. Technol. 209 (2009) 1853–1860, https://doi.org/10.1016/j.jmatprotec.2008.04.034.
[46] Z.M. Al-Rashidy, M.M. Farag, A.N.A. Ghany, A.M. Ibrahim, W.I. Abdel-Fattah, Orthopaedic bioactive glass/chitosan composites coated 316L stainless steel by green electrophoretic co-deposition, Surf. Coat. Technol. 334 (2018) 479–490, https://doi.org/10.1016/j.surfcoat.2017.11.052.
[47] M. Alaei, M. Atapour, S. Labbaf, Electrophoretic deposition of chitosan-bioactive glass nanocomposite coatings on AZ91 Mg alloy for biomedical applications, Prog. Org. Coat. 147 (2020), 105803, https://doi.org/10.1016/j.porgcoat.2020.105803.
[48] E. Kontonasaki, T. Zorba, L. Papadopoulou, E. Pavlidou, X. Chatzistavrou, K. Paraskevopoulos, P. Koidis, Hydroxy carbonate apatite formation on particulate bioglass in vitro as a function of time, Cryst. Res. Technol. 37 (2002) 1165–1171, https://doi.org/10.1002/1521-4079(200211)37:11<1165::AID-CRAT1165>3.0.CO;2-R.
[49] K. Zheng, A. Solodovnyk, W. Li, O.M. Goudouri, C. Stahli, S.N. Nazhat, A. R. Boccaccini, Aging time and temperature effects on the structure and bioactivity of gel-derived 45S5 glass-ceramics, J. Am. Ceram. Soc. 98 (2015) 30–38, https://doi.org/10.1111/jace.13258.
[50] A. Pawlak, M. Mucha, Thermogravimetric and FTIR studies of chitosan blends, Thermochim. Acta 396 (2003) 153–166, https://doi.org/10.1016/S0040-6031(02)00523-3.
[51] J. Kumirska, M. Czerwicka, Z. Kaczynski, A. Bychowska, K. Brzozowski, J. Thoming, P. Stepowski, Application of spectroscopic methods for structural analysis of chitin and chitosan, Mar. Drugs 8 (2010) 1567–1636, https://doi.org/10.3390/md8051567.
[52] V.F. Lvovich, Impedance Spectroscopy: Applications to Electrochemical and Dielectric Phenomena, Wiley, Somerset, NJ, USA, 2012.
[53] H. Wilda, J.E. Gough, In vitro studies of annulus fibrosus disc cell attachment, differentiation and matrix production on PDLLA/45S5 Bioglass composite films, Biomaterials 27 (2006) 5220–5229, https://doi.org/10.1016/j.biomaterials.2006.06.008.
[54] K.L. Menzies, L. Jones, The impact of contact angle on the biocompatibility of biomaterials, Optom. Vis. Sci. 87 (2010) 387–399, https://doi.org/10.1097/OPX.0b013e3181da863e.
[55] Y. Tamada, Y. Ikada, Cell adhesion to plasma-treated polymer surfaces, Polymer 34 (1993) 2208–2212, https://doi.org/10.1016/0032-3861(93)90752-V.
[56] J.H. Lee, G. Khang, J.W. Lee, H.B. Lee, Interaction of different types of cells on polymer surfaces with wettability gradient, J. Colloid Interface Sci. 205 (1998) 323–330, https://doi.org/10.1006/jcis.1998.5688.
[57] R. Rej, J.P. Bretaudiere, Effects of metal ions on the measurement of alkaline phosphatase activity, Clin. Chem. 26 (1980) 423–428, https://doi.org/10.1093/clinchem/26.3.423.
[58] X.N. Gu, N. Li, Y.F. Zheng, L. Ruan, In vitro degradation performance and biological response of a Mg-Zn-Zr alloy, Mater. Sci. Eng. B Solid Mater. Adv. Technol. 176 (2011) 1778–1784, https://doi.org/10.1016/j.mseb.2011.05.032.
[59] M. Cerruti, D. Greenspan, K. Powers, Effect of pH and ionic strength on the reactivity of Bioglass® 45S5, Biomaterials 26 (2005) 1665–1674, https://doi.org/10.1016/j.biomaterials.2004.07.009.
[60] A.L. Macon, T.B. Kim, E.M. Valliant, K. Goetschius, R.K. Brow, D.E. Day, A. Hoppe, A.R. Boccaccini, I.Y. Kim, C. Ohtsuki, T. Kokubo, A. Osaka, M. Vallet-Regi, D. Arcos, L. Fraile, A.J. Salinas, A.V. Teixeira, Y. Vueva, R.M. Almeida, M. Miola, C. Vitale-Brovarone, E. Verne, W. Holand, J.R. Jones, A unified in vitro evaluation for apatite-forming ability of bioactive glasses and their variants, J. Mater. Sci. Mater. Med. 26 (2015) 115, https://doi.org/10.1007/s10856-015-5403-9.